Journal of Molecular Liquids 436 (2025) 128240

Contents lists available at ScienceDirect

Journal of Molecular Liquids

journal homepage: www.elsevier.com/locate/molliq

Investigation of the phase behavior of an aqueous solution comprising anionic and cationic surfactant mixtures

Mukesh Chandra Bos [a], Shallu Dhingra [b], Manoj Kumar Srivastava [c], Priyanka Sharma [a], Santanu Kumar Pal [b,*], Santosh Prasad Gupta [a,*]

[a] Department of Physics, Patna University, Patna, 800005, Bihar, India
[b] Department of Chemical Sciences, Indian Institute of Science Education and Research (IISER) Mohali, Sector-81, SAS Nagar, Knowledge City, Manauli, Mohali, 140306, Punjab, India
[c] Department of Physics, D. A. V. P. G. College, Gorakhpur, 273001, U. P., India

ARTICLE INFO

Keywords:
Surfactant
CPC
SDS
H phase
N_d phase
L_α^D phase
L_α phase

ABSTRACT

In this study, we examined the influence of an anionic surfactant, specifically sodium dodecyl sulfate (SDS), on the phase behavior of aqueous solutions containing a cationic surfactant, cetylpyridinium chloride (CPC). In particular, the phase behavior of the CPC-SDS-water system has been examined at different molar ratios of [SDS]/[CPC] and a constant weight fraction (in percentage) of CPC + SDS in water ($\Phi_s = 50$) along with a constant temperature ($T = 50\,^{\circ}C$), employing small angle X-ray scattering (SAXS) and polarizing optical microscopy (POM) techniques. With rising SDS concentration, the system displays four phases: hexagonal (H), a nematic phase of disk-shaped micelles (N_d), a random mesh phase (L_α^D), and lamellar (L_α) phase. The two phases, L_α^D and L_α, exist together with excess water, leading to denote as $I + L_\alpha^D$ and $I + L_\alpha$, correspondingly. Electron density maps have been reconstructed for the H and L_α phases. The L_α phase observed at elevated SDS concentrations is characterized as a short-range disordered L_α phase. The L_α phase and the disordered L_α phase are effectively depicted by the L_α phase model provided by Pabst et al. We have further detailed the phase behavior of the CPC-SDS-water system at $\alpha = 0.9$, T = 50 °C, and Φ_s 30, 39, 50, 60, 68, and 79 to study the swelling behavior of the bilayer structure in the pure L_α which has been found to be in agreement with swelling behavior of the bilayer structure.

1. Introduction

Surfactants are classified as amphiphiles, which are a category of organic chemical entities that possess both hydrophilic and hydrophobic moieties in varying proportions and configurations. They exhibit surface stabilizing capabilities that facilitates the adsorption of surfactants at interfaces and allows for self-assembly into various micellar aggregations above a certain concentration. This specific concentration is referred to as the critical micellar concentration (CMC) [1,2]. Surfactants are capable of performing numerous diverse functions, including wetting, emulsification, solubilization, dispersion, and foaming, in addition to cleaning; moreover, they can also be quite beneficial for enhancing penetration and antimicrobial activity. Their remarkable functional diversity has led to their application in the production and processing of food, agrochemicals, pharmaceuticals, personal care products, laundry products, and petroleum. Amphiphiles such as peptides are utilized in tissue and cell engineering, antimicrobials, drug delivery systems, and other biomedical applications due to their exceptional biocompatibility [3–5].

The phase diagrams of single-chain surfactants are predominantly characterized by the hexagonal (H_I) phase, which comprises cylindrical micelles organized on a two-dimensional (2D) hexagonal lattice and exists over a broad spectrum of concentration. At even greater concentrations, a lamellar (L_α) phase is observed, consisting of a repetitive stack of planar amphiphile bilayers that are interspersed with water. An additional increase in concentration leads to the formation of inverse structures, wherein water-filled regions, surrounded by the hydrophilic head groups of the amphiphilic molecules, are dispersed within the hydrocarbon matrix. These inverse micellar morphologies are designated as type II, while the direct micellar morphologies are referred to as type I.

* Corresponding authors.
E-mail addresses: skpal@iisermohali.ac.in, santanupal.20@gmail.com (S.K. Pal), santosh-phy@patnauniversity.ac.in, drspgpu@gmail.com (S.P. Gupta).

https://doi.org/10.1016/j.molliq.2025.128240
Received 13 January 2025; Received in revised form 21 July 2025; Accepted 29 July 2025

Available online 6 August 2025

Numerous studies suggest that the morphological shift from cylinders to bilayers does not occur suddenly, but rather through a series of intermediate shapes, resulting in a sequence of so-called intermediate phases lying between the hexagonal and lamellar phases [6–12]. Intermediate phases can be classified into three categories: bicontinuous cubic phases, ribbon phases, and mesh phases; all of which can manifest as type I and type II. Mesh phases consist of 2D, mesh-like aggregates, which may also be characterized as bilayers featuring a regular arrangement of monodisperse pores [8,10–12]. In the ordered mesh phases, the mesh-like aggregates lock into a three-dimensional lattice. Conversely, the random mesh phase (L_{α}^{D}) is characterized by a periodic stacking of these aggregates, lacking long-range positional correlations of the in-plane structure; this phase can also be referred to as a lamellar phase with in-plane defects that show weak correlation [9–11].

In this context, the organic salts, including 2-sodium-3-hydroxy naphthoate (SHN) and p-toluidine hydrochloride (PTHC), represent compounds that can be regarded as an extreme example of ionic surfactants, referred to as 'hydrotropes'. These substances are incapable of forming micelles independently in water; however, in the presence of surfactants, they preferentially position themselves at the water-micellar interface, thereby influencing the characteristics of the curvature of the micelle-water interface, resulting in a variety of structures even at low surfactant concentrations in aqueous media. In numerous amphiphiles, this reduction is sufficiently significant to trigger the formation of elongated, worm-like micelles (WLM), as demonstrated by studies referenced in the literature [10,12]. Moreover, bilayers have been noted to achieve stability under specific conditions, particularly when there is a substantial decrease in the spontaneous curvature [8,10,12]. These bilayers typically exhibit a tendency to curl up, resulting in the formation of both multi-lamellar and uni-lamellar vesicles.

The aqueous solution of the combination of surfactants constitutes a well-established system for the production of uni-lamellar vesicles (ULVs) intended for use as carriers in drug delivery. The mixtures typically consist of anionic/anionic, cationic/cationic, nonionic/nonionic, amphoteric/amphoteric, anionic/nonionic, cationic/nonionic, or amphoteric/nonionic surfactants. Nevertheless, synergism increases as the degree of charge disparity increases [13,14], indicating that the synergism between anionic/anionic or nonionic/nonionic is less significant than that observed between anionic/nonionic or cationic/ nonionic, which is, in turn, less than that observed between cationic/anionic. Therefore, the greatest synergism is achieved by combining anionic and cationic surfactants; thus, a more comprehensive understanding of this system may expand the potential for formulating the ULVs.

Mixtures of anionic and cationic surfactants exhibit numerous distinctive properties: they possess significantly lower CMC than individual pure surfactants; they are typically more surface-active than any single pure surfactant; and they can create microstructures not formed by pure components. Additionally, they have the capability to reduce the concentration necessary for the formation of liquid crystalline phases. The equimolar composition of anionic and cationic surfactants, collectively referred to as a 'catanionic' system, displays a bilayer structure [15,16].

In the present article, we examine the phase behavior of aqueous solutions comprising the anionic surfactant sodium dodecyl sulfate (SDS) and the cationic surfactant cetylpyridinium chloride (CPC). SDS has garnered considerable attention in research, which has led to the identification of several intermediate phases within its system, encompassing ribbon, ordered mesh, bicontinuous cubic phases; and hexagonal (H) phase, along with lamellar (L_{α}) phases. Nevertheless, these intermediate phases are predominantly observed within a narrow range of compositions [17]. Conversely, CPC is a cationic quaternary ammonium compound utilized in certain varieties of mouthwashes, toothpastes, lozenges, throat sprays, breath sprays, and nasal sprays. It functions as an antiseptic effective at eliminating bacteria and other microorganisms. Generally, the aqueous solution of CPC is characterized by a predominance of hexagonal phases composed of cylindrical micelles and also contains a nematic phase of rod-like micelles [18].

In the present study, the phase behavior of the CPC-SDS-water system at various molar ratios (α) of [SDS]/[CPC] and at a constant weight fraction (in percentage) of CPC + SDS in water ($\Phi_s = 50$) and a fixed temperature ($T = 50\,^{\circ}\mathrm{C}$) is presented. Polarizing optical microscopy (POM) and small angle X-ray scattering (SAXS) techniques are employed to delineate the distinct phases exhibited by the CPC-SDS-water system. The system reveals a series of phases, specifically identified as hexagonal (H) phase, nematic phase of disk-like micelles (N_d), random mesh phase (L_{α}^{D}), as well as L_{α} phases, which manifest in response to increasing SDS concentration. It has been noted that both the phases; L_{α}^{D} and L_{α}, coexist with excess water, resulting, these phases are referred to as $I + L_{\alpha}^{D}$ and $I + L_{\alpha}$, respectively. Interestingly, the L_{α} phase observed at elevated concentrations of SDS is characterized by short-range positional order and is termed as a disordered L_{α} phase. In this investigation, the L_{α} phase was modeled by employing the methodology outlined by Pabst et al. [19]. The article is structured as follows: it first gives the details about the materials and methods utilized, then presents the results, and concludes with a comprehensive analysis of the findings.

2. Materials and methods

The surfactants, CPC and SDS, with more than 99% purity, were procured from Sigma-Aldrich and used without further purification, the chemical structure is shown in the figure [supporting Figure S1]. The samples were prepared by adding the deionized water (Millipore) to the mixture of these two surfactants at appropriate concentration. The molar ratio ($\alpha = [SDS]/[CPC]$) of these two surfactants were varied from 0 to 1.6 in increments of 0.2. The total weight fraction (in percentage), Φ_s, of surfactants, $CPC + SDS$, ($\Phi_s = \frac{(CPC+SDS)x100}{CPC+SDS+Water}$), dissolved in water was maintained at fixed value that is $\Phi_s = 50$. Subsequently, the samples were enclosed in tubes, sealed, and allowed to incubate for a duration exceeding a week at a temperature of 50 °C.

For the purpose of POM observations under crossed polarizers, the samples were kept between a glass slide and a cover slip. The observations of textures corresponding to the mesophase were performed with Nikon Eclipse LV100POL polarizing optical microscope provided with a Linkam heating stage (LTS 420). All images were captured using a Q-imaging camera. It was noted that phase changes were monitored only for the region closely to the center of the sample, away from its edges.

In the SAXS experiments, the samples were kept within glass capillaries (Hampton Research), each with a diameter of 0.7 mm, then they were sealed with a flame. When these tubes were filled, it was noticed that some materials aligned due to shear flow. For the SAXS experiment, we utilized the GeniX 3D setup. The X-ray radiation was obtained from a shield tube anode X-ray source (provided by Xenocs), which was equipped with a multi-layer mirror for collimation. This apparatus functioned at a voltage of 50 kV and applied a current of 0.6 mA to generate fine X-ray beam. The information from these patterns was recorded using a two-dimensional Pilatus detector, noted for its pixel size of 172 μm x 172 μm. The duration of each scan ranged from 20 to 90 minutes. The ability to accurately measure the spacing of the small-angle sharp peaks in the diffraction patterns was remarkable, with an accuracy of 0.03 nm. However, the accuracy in determining the spacing of the diffuse peaks was somewhat limited, with an accuracy of 0.1 nm.

Correlation length corresponding to different phases is calculated to gain insights into the order of the observed phases. The formula $\xi = \frac{2\pi k}{\Delta q}$ is utilized to calculate the correlation length, which corresponds to the extent of order within mesophases. This equation is analogous to Scherrer's formula, $\xi = \frac{\lambda k}{\Delta(2\theta)Cos\theta}$, where θ represents the position of the peak in radians, λ denotes the wavelength of the incident X-ray, $\Delta(2\theta)$ characterizes the broadening at half the maximum intensity (Full Width Half Maximum, FWHM) in radians, and k is a shape factor, typically valued at 0.89. The scattering wave vector q is defined as $q = \frac{4\pi Sin\theta}{\lambda}$, and the broadening of q at half the maximum intensity is referred to as Δq. Applying a Lorentzian curve to the first strong peak of different phases

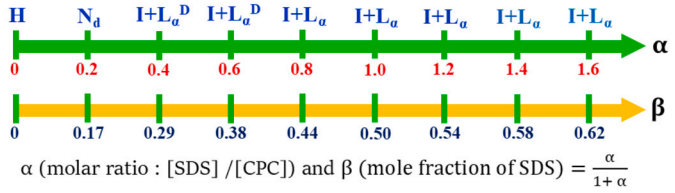

Fig. 1. Phase behavior of CPC-SDS-water system at $T = 50\,°C$, $\Phi_s = 50$, and at various values of molar ratio, $\alpha = [SDS]/[CPC]$. H, N_d, L_α^D, L_α and I denote hexagonal phase, nematic phase of disk like micelles, lamellar phase, and isotropic phase due to excess water, respectively. The same phase diagram is illustrated in relation to the mole fraction of SDS, designated as β, where β can be defined as $\beta = \frac{\alpha}{1+\alpha}$.

within their SAXS pattern results in the determination of the peak position, represented as q, along with the corresponding Δq value associated with that phase. Furthermore, the correlation length is typically scaled relative to the lattice parameter, thereby providing a measure of the spatial length scale of correlation in relation to the dimensions of the molecular length scale. This results in a dimensionless value, denoted as $\frac{\xi}{lp}$ (where lp is the lattice parameter), which is essential for facilitating comparison.

For a deeper understanding of the electronic distribution within the H and L_α phases, an electron density map associated with these phases has been further reconstructed by using procedures as described by S. P. Gupta et al. [20]. By employing the method of inverse Fourier transformation, the scattering amplitude, denoted by $F_s(hkl)$, of a liquid-crystalline (mesophase) phase is linked to its electron density profile, represented by $\rho(x, y, z)$ as;

$$\rho(x, y, z) = \sum_{hkl} F_s(hkl) e^{2\pi i(hx+ky+lz)} \tag{1}$$

In the given formula, (hkl) represents the Miller indices of the planes corresponding various reflected peaks observed in SAXS pattern's of the phases, while x, y, and z denote the fractional coordinates within the unit cell. The scattering amplitude, denoted by $F_s(hkl)$, is a complex quantity. It can be expressed as the product of its phase, $\Phi(hkl)$, and its magnitude, which is denoted as $|F_s(hkl)|$. The magnitude $|F_s(hkl)|$ exhibits a direct proportionality to the square root of the intensity, $I(hkl)$, of the reflected X-ray radiation. That is;

$$F_s(hkl) = |F_s(hkl)| e^{\Phi(hkl)} = \sqrt{I(hkl)} e^{\Phi(hkl)} \tag{2}$$

To ascertain the intensities of the distinct peaks observed in various phases in their SAXS pattern, one proceeds by computing the area beneath each peak following the subtraction of the background, and applying the requisite geometric and multiplicity adjustments. For each diffraction peak, the phase variable $\Phi(hkl)$ stands alone as the information that cannot be directly retrieved from the SAXS experiment. However, when the structure under investigation is centrosymmetric, this issue becomes amenable to solution, indicating that $\Phi(hkl)$ may only assume values of 0 or π. This is justified by the fact that scattering amplitude, $F_s(hkl)$, can only be real if the electron density distribution profile is centro-symmetric that is $\rho(-x, -y, -z) = \rho(x, y, z)$. Consequently, any phase value ranging from 0 to 2π can represent the phase for non-centro-symmetric groups. Given that the phases H and L_α that have been observed are centro-symmetric, the process of reconstructing electron density maps becomes a straightforward endeavor. This involves interpreting the phase variable $\Phi(hkl)$ as either 0 or π. Subsequently, the most appropriate map is determined based on the quality of the reconstructed electron density maps, alongside additional physical and chemical data pertaining to the system, such as the size and composition of the constituent chemical species.

3. Results and discussion

The phase behavior of the CPC-SDS-water system at the temperature $T = 50\,°C$, $\Phi_s = 50$, and at various values of α, is represented in figure [Fig. 1]. The equilibrium of water at the weight concentration represented by $\Phi_s = 50$ enhances the opportunity to gain valuable information regarding phase behavior, additionally, the mixture of CPC and SDS crystallizes at temperatures below 50 °C; therefore, we have chosen to perform the experiments at fixed temperature 50 °C and $\Phi_s = 50$. The existence of different phases at various compositions is confirmed by the through analysis of their SAXS patterns, supported by POM texture. At lower α values, the system exhibit H phase. Furthermore, the N_d phase and L_α^D show stabilization on further increasing the α values. However, the L_α phase is found to be stable at higher values of α. However, the correlation within the L_α phases decreases with increasing the α values. The correlation has been calculated by utilizing the procedure as discussed in the section [Section 2]. It is observed that an excess of water coexists within the L_α^D and L_α phases, thus classifying the phase as $I + L_\alpha^D$ and $I + L_\alpha$, respectively. The sequence of phase transitions is found to be $H \rightarrow N_d \rightarrow I + L_\alpha^D \rightarrow I + L_\alpha$, with a progressive increase in α. A comprehensive analysis of this phase behavior is provided below.

In the present study, we aim to describe the phase behavior of the CPC-SDS-water system with fixed parameters of $\Phi_s = 50$ and $T = 50\,°C$, while varying the values of α. Initially, we examined the self-assembled structure of pure SDS in aqueous media as a reference point. The aqueous solution of pure SDS at $\Phi_s = 50$ and $T = 50\,°C$ exhibits a viscous consistency and presents a smooth texture under crossed POM [Fig. 2A]. Additionally, the associated SAXS pattern reveals two distinct quasi-Bragg peaks in the small-angle region, with d-spacing ratios of 1: $\frac{1}{\sqrt{3}}$. These peaks correspond to reflections from the (100) and (110) planes of a two-dimensional hexagonal lattice, respectively [Figs. 3A (a) and 4A]. The d-spacings have been calculated using the relation $d_{hkl} = \frac{\sqrt{3}a}{2\sqrt{h^2+hk+k^2}}$. The calculated lattice parameter is determined to be $a = 48.98$ Å. Furthermore, the correlation length, ξ, associated with the (100) peak has been found to be approximately 1030 Å, which corresponds to around 21 correlated cylindrical micelles (columns) along the columnar plane of the H phase. This finding indicates a quasi-long-range positional order within this phase [Table 1].

The CPC-SDS-water system at $\alpha = 0.0$ (representing the pure CPC in aqueous media) demonstrates significant viscosity and exhibits a smooth texture when observed under crossed polarizers [Fig. 2B], the associated SAXS pattern reveals two distinct quasi-Bragg peaks within the small angle region, exhibiting d-spacing ratios of $1 : \frac{1}{\sqrt{3}}$. These peaks correspond to reflections from the (100) and (110) planes of the two-dimensional hexagonal lattice, as illustrated in Figs. 3A (b) and 4B. The calculated lattice parameter is determined to be $a = 54.63$ Å, as presented in Table 1. The POM texture, in conjunction with the SAXS pattern, indicates that the micelles possess cylindrical shapes on average and are organized within a two-dimensional hexagonal lattice at this composition, resulting in the establishment of a hexagonal (H) phase. Furthermore, the calculated correlation length is approximately 1271 Å, corresponding to around 23 correlated cylindrical columns along the columnar plane of the H phase, thereby confirming a quasi-long range periodic arrangement within the phase.

Furthermore, the CPC-SDS-water system at $\alpha = 0.2$ show lower viscosity as compared with that observed at $\alpha = 0$, exhibiting schlieren texture along with pseudo isotropic areas, where the optic axis is perpendicular to the bounding plates, under crossed polarizers [Fig. 2C], suggesting the nematic (N_d) phase, composed of micelles that have a disk-like shape which are also known as 'bicelles'. Additionally, the corresponding SAXS pattern reveals a single non-Bragg's broad peak in the small angle region with an average d-spacing of 54.73 Å, alongside a secondary very diffuse peak with d-spacing precisely half of the first as indicated by the black bar on the SAXS curve, demonstrating short-range

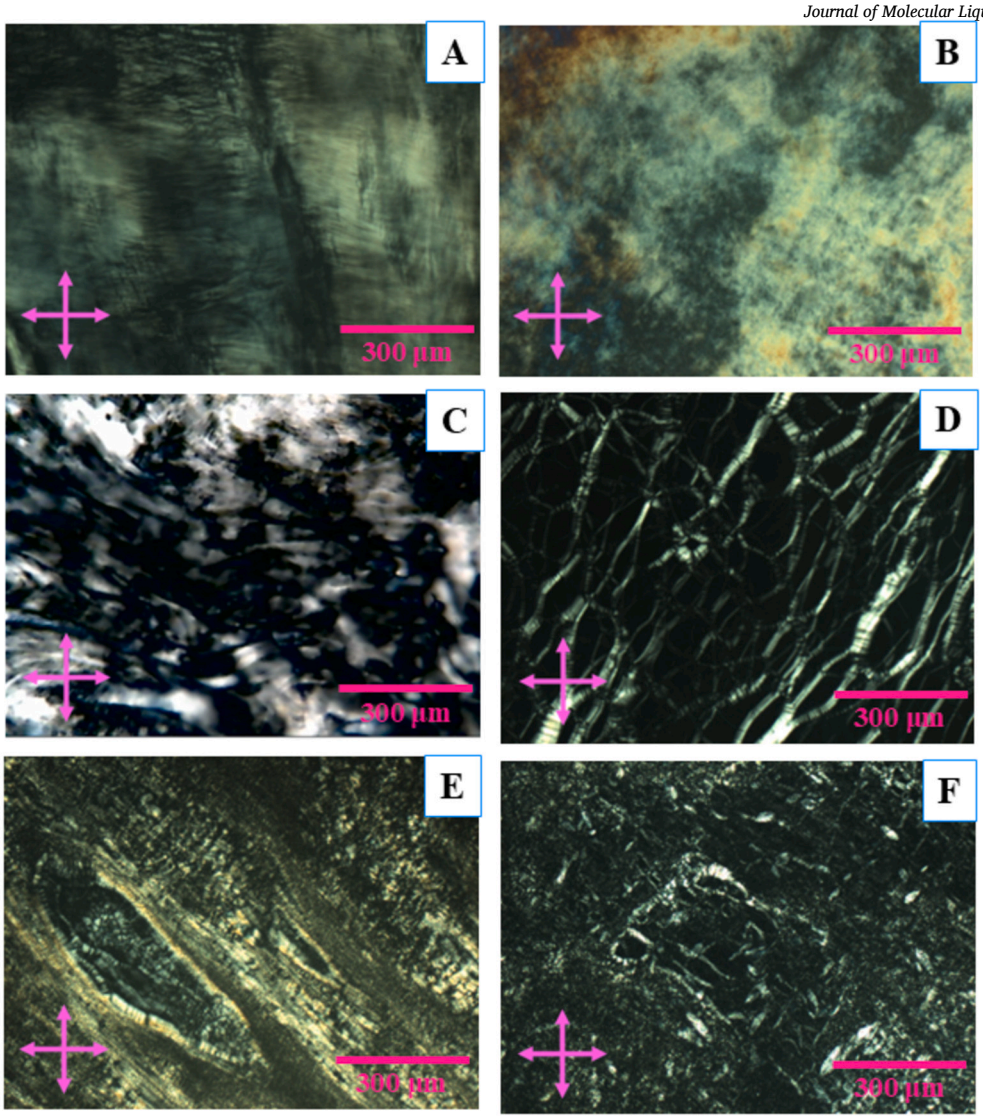

Fig. 2. Polarizing optical microscopy (POM) textures (under crossed polarizers) of (A) H phase exhibited by pure SDS-water system at $\Phi_s = 50$ & $T = 50\,^{\circ}\mathrm{C}$. POM texture of CPC-SDS-water system at $\Phi_s = 50$ & $T = 50\,^{\circ}\mathrm{C}$ of: (B) H phase at $\alpha = 0.0$, (C) N_d phase at $\alpha = 0.2$, (D) L_{α}^{D} phase at $\alpha = 0.4$, (E) L_{α}^{D} phase at $\alpha = 0.6$ and (E) L_{α} phase at $\alpha = 0.8$. H, N_d, L_{α}^{D} and L_{α} denote the hexagonal phase, nematic phase of disk like micelles, random mesh phase and lamellar phases, respectively. The L_{α}^{D} and L_{α} phase found to be coexist with excess water which show black region under crossed POM.

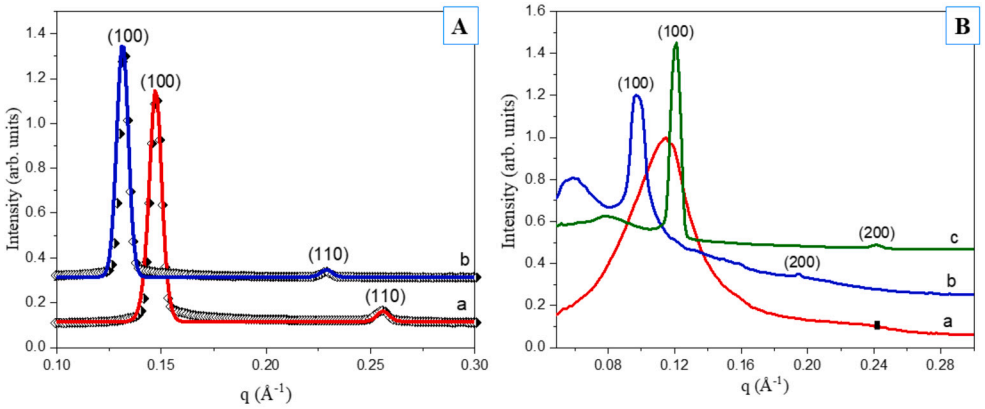

Fig. 3. Small angle X-ray scattering data of the CPC-SDS-water system at $\Phi_s = 50$, $T = 50\,^{\circ}\mathrm{C}$ exhibits: (A) (a) H phase (pure SDS-water system) at $\Phi_s = 50$, $T = 50\,^{\circ}\mathrm{C}$, the data is shown by half-filled diamond in black color along with fit, the curve in red color, (b) H phase at $\alpha = 0.0$, the data is shown by half-filled diamond in black color along with fit, the curve in blue color. (B) (a) N_d phase at $\alpha = 0.2$, curve in red color. The phase exhibits a very diffuse peak with spacing $\frac{1}{2}$ of the first peak denoted by black bar on the curve, due to short-range lamellar order of the disk-like micelles, (b) L_{α}^{D} phase at $\alpha = 0.4$, curve in blue color, (c) L_{α}^{D} phase at $\alpha = 0.6$, curve in green color. H, N_d and L_{α}^{D} denote the hexagonal phase, nematic phase of disk like micelles and random mesh phase, respectively. The L_{α}^{D} phase found to be coexist with excess water.

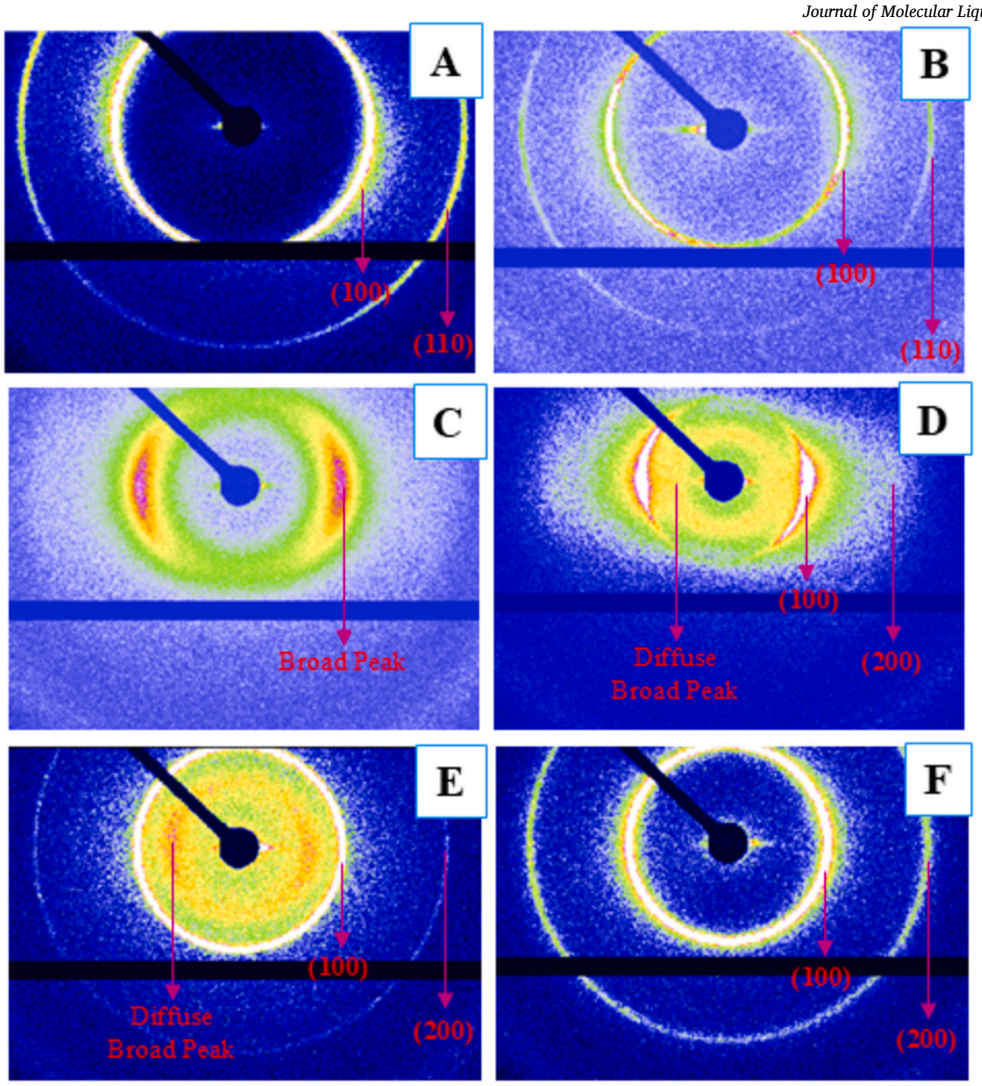

Fig. 4. Two-dimensional Small angle X-ray scattering data of the CPC-SDS-water system at $\Phi_s = 50$, $T = 50\,^{\circ}C$ exhibits: (A) H phase (pure SDS-water system at $\Phi_s = 50$, $T = 50\,^{\circ}C$), (B) H phase at $\alpha = 0.0$, (C) N_d phase at $\alpha = 0.2$, (D) L_{α}^{D} phase at $\alpha = 0.4$, (E) L_{α}^{D} phase at $\alpha = 0.6$ and (F) L_{α} phase at $\alpha = 0.8$. H, N_d, L_{α}^{D} and L_{α} denote the hexagonal phase, nematic phase of disk like micelles, random mesh phase and lamellar phases, respectively. The L_{α}^{D} and L_{α} phase found to be coexist with excess water.

lamellar order, thus confirming the presence of the N_d phase [Figs. 3B (a) and 4C & Table 1]. The computed correlation length is determined to be approximately 143 $\AA$, which corresponds to around 3 correlated disks along the disk plane. Such a limited number of correlated units confirms a very short range positional order within the phase, which is characteristic of the N_d phase.

Furthermore, the CPC-SDS-water system at $\alpha = 0.4$ and 0.6 exhibits an oily texture accompanied by a maltese cross, which is indicative of layered structure of bilayers along with multi-lamellar vesicles [Fig. 2D and Fig. 2E]; the corresponding SAXS pattern displays one non-Bragg's diffuse peak in the small angle region in addition to two sharp Bragg's peaks [Figs. 3B (b, c) and 4D and 4E]. The d-spacing of the sharp peaks is observed to be in the ratio of $1 : \frac{1}{2}$, thereby confirming the presence of a layered structure of bilayers; however, the diffuse peak arises from the correlations of the defects within the bilayers along the plane of bilayers, confirming the existence of a random mesh phase (L_{α}^{D}) [Table 1]. The lamellar periodicity, d, is determined to be 64.91 $\AA$ and 51.84 $\AA$ at $\alpha = 0.4$ and $\alpha = 0.6$, respectively. Additionally, the d spacing corresponding to the diffuse peak, d_d, is found to be 105.42 $\AA$ and 79.63 $\AA$ at $\alpha = 0.4$ and $\alpha = 0.6$, respectively. Furthermore, the correlation length, calculated corresponding to the (100) peak, is found to be approximately 608 $\AA$ and 986 $\AA$, at $\alpha = 0.4$ and $\alpha = 0.6$, corresponding to approximately 9 and 19 correlated defected bilayers along the normal to the plane of the bilayer, respectively [Table 1].

Furthermore, the CPC-SDS-water system at $\alpha = 0.8$ demonstrates an oily texture along with maltese crosses, indicative of a layered bilayer structure with multi-lamellar vesicles [Fig. 2F] as discussed above. The corresponding SAXS pattern does not exhibit diffuse peak in the small angle region but displays two sharp Bragg's peaks with d-spacing in the $1 : \frac{1}{2}$ ratio, which correspond to the reflections from the (100) and (200) planes of the one-dimensional lattice, respectively, confirming the occurrence of the L_{α} phase, composed of bilayers arranged on a one-dimensional lattice separated by a water layers [Figs. 6(a) and 4F]. The calculated lamellar periodicity, d, is determined to be 54.18 $\AA$ [Table 1]. Similarly, the CPC-SDS-water system at $\alpha = 1.0,\ 1.2,\ 1.4$ & 1.6 exhibits the L_{α} phase [5A, 5B, 5C, 5D and 6 (b,c,d,e) and 7A, 7B, 7C & 7D]. The lamellar periodicity in all these compositions is found to be approximately 55 $\AA$. However, the correlation length is found to be approximately 922 $\AA$, 832 $\AA$, 589 $\AA$, 181 $\AA$, and 185 $\AA$ corresponding to about 17, 14, 9, 3, and 3 numbers of correlated bilayers perpendicular to the bilayer plane at $\alpha = 0.8, 1.0, 1.2, 1.4$ and 1.6, respectively [Table 1]. The correlated number of bilayers unit at $\alpha = 1.4$ and 1.6 are about 3 which indicative of a very short positional order within this phase, confirming that, the observed L_{α} phase at this composition is

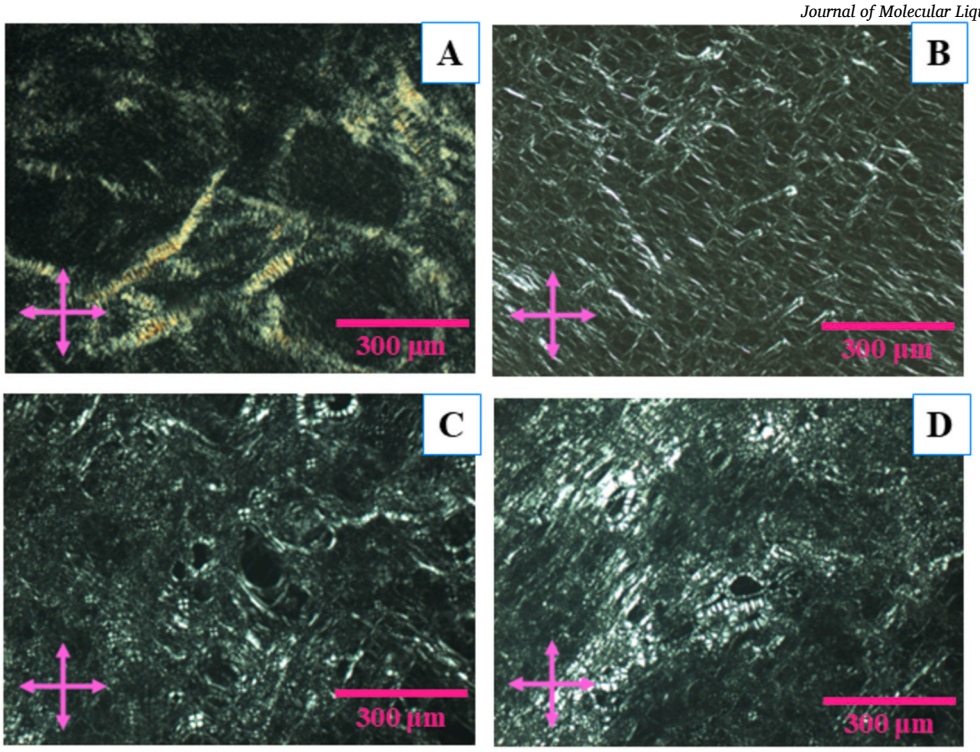

Fig. 5. Polarizing optical microscopy textures (under crossed polarizers) of L_α phase of CPC-SDS-water system at $\Phi_s = 50$ & $T = 50\,°C$ and (A) $\alpha = 1.0$, (B) $\alpha = 1.2$, (C) $\alpha = 1.4$ and (A) $\alpha = 1.6$. The L_α phase found to be coexist with excess water which show black region under crossed POM.

Table 1
The table exhibits the observed and calculated d-spacings, Miller indices, intensities, phases values for the various phases as well as the variation of correlation length, ξ and no. of correlated units (ξ/lp) in the various phases observed in CPC-SDS-water system at $\Phi_s = 50$ and T = 50 °C. a is the lattice parameter of the H phase, d is lamellar periodicity of the $I + L_\alpha$ and $I + L_\alpha^D$ phase, d_d is the spacing of the diffuse peak in the $I + L_\alpha^D$ phase and as is the average spacing between the disk like micelles along the disk plane. lp is equivalent to a or d or as.

α	$a/d/d_d/as$ (Å)	Miller indices (hkl)	d_{obs} (Å)	d_{cal} (Å)	Relative Intensity	Multi-plicity	Φ (hkl)	Phase	ξ (approx.) (Å)	(ξ/lp) (approx.)
Pure SDS	a = 48.98	(100)	42.42	42.42	100.00	6	π	H	1030	21
		(110)	24.55	24.49	4.23	6	π			
0.0	a = 54.63	(100)	47.31	47.31	100.00	6	π	H	1271	23
		(110)	27.45	27.31	3.81	6	π			
0.2	as =54.73	as	54.73	-	-	-	-	N_d	143	3
0.4	d_d =105.42	d_d	105.42	-	-	-	–	$I + L_\alpha^D$		
	d = 64.91	(100)	64.91	64.91	-	-	-		608	9
		(200)	32.34	32.45	-	-	-			
0.6	d_d =79.63	d_d	79.63	-	-	-	–	$I + L_\alpha^D$		
	d = 51.84	(100)	51.84	51.84	-	-	-		986	19
		(200)	25.98	25.92	-	-	-			
0.8	d = 54.18	(100)	54.18	54.18	100.00	2	π	$I + L_\alpha$	921	17
		(200)	27.11	27.09	7.01	2	π			
1.0	d = 59.13	(100)	59.13	59.13	100.00	2	π	$I + L_\alpha$	832	14
		(200)	29.59	29.56	7.13	2	π			
1.2	d = 64.05	(100)	64.05	64.05	-	-	-	$I + L_\alpha$	588	9
		(200)	31.98	32.02	-	-	-			
1.4	d = 57.50	(100)	57.50	57.50	-	-	-	$I + L_\alpha$	181	3
		(200)	28.72	28.75	-	-	-			
1.6	d = 58.30	(100)	58.30	58.30	-	-	-	$I + L_\alpha$	185	3
		(200)	29.12	29.15	-	-	-			

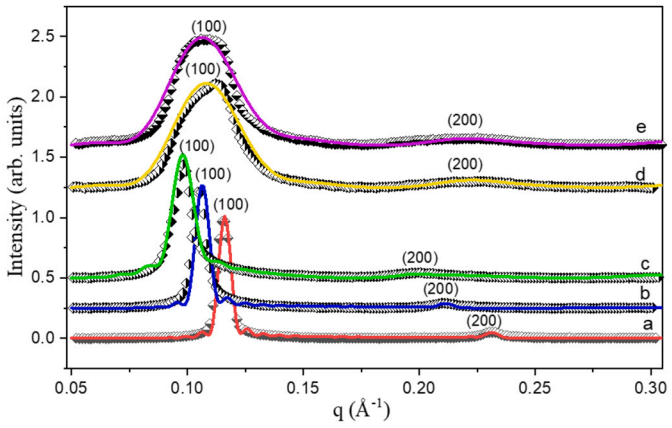

Fig. 6. Small angle X-ray scattering data of the CPC-SDS-water of L_α phase of CPC-SDS-water system at $\Phi_s = 50$ & $T = 50\,°C$ along with fit to the model of L_α phase proposed by Pabst et al. The data is shown by half-filled diamond in black color and (a) L_α phase at $\alpha = 0.8$ along with fit, the curve in red color, (b) L_α phase at $\alpha = 1.0$ along with fit, the curve in blue color, (c) L_α phase at $\alpha = 1.2$ along with fit, the curve in green color, (d) L_α phase at $\alpha = 1.4$ along with fit, the curve in yellow color and (e) L_α phase at $\alpha = 1.6$ along with fit, the curve in purple color. The L_α phase found to be coexist with excess water.

disordered and very close in structure to the novel isotropic phase of bilayer (L_x phase) as discussed in the reference [21]. However, the L_α phase at α = 0.8, 1.0, and 1.2 is typically stable and possesses an ordered structure.

For a more profound comprehension of the electronic desity distribution within the H and L_α phases, an electron density map corresponding to these phases has been additionally reconstructed utilizing the procedures outlined by S. P. Gupta et al. [20] and briefly presented in the Materials and Methods section [Section 2]; the characteristics of these reconstructed maps are detailed below. The electron density maps have been reconstructed for the H phase observed in the aqueous solution of SDS and CPC ($\alpha = 0.0$) at $\Phi_s = 50$ and $T = 50\,°C$, as well as for the stable ordered L_α phase observed at $\alpha = 0.8$ and 1.0.

Fig. 8(A, B) illustrates the reconstructed electron density maps for the H phase, which were recorded for pure SDS and pure CPC ($\alpha = 0.0$) at $\Phi_s = 50$, and $T = 50\,°C$, respectively. These reconstructed electron density maps are based on the data obtained from the X-ray diffraction pattern of these phases such as the Miller indexing of peaks of the phase, encompassing their intensities, multiplicities, and phase factors as detailed in table [Table 1]. In the map, the regions of highest electron density are highlighted in deep red, whereas those depicted in deep blue represent the regions of lowest electron density. The presented maps demonstrate a two-dimensional (2D) hexagonal lattice configuration, where areas of low electron density exhibit 2D hexagonal lattice distributed in the high electron density matrix, the low electron density region correspond to the alkyl chain of the CPC-SDS-water system.

The reconstructed electron density maps for the L_α phase at the compositions, $\alpha = 0.8$ and 1, have been presented in the figure [Fig. 8(C, D)], the associated parameters which are used to construct these maps such as peak intensity, Miller indices, multiplicity, and phase of the peak, are outlined in the accompanying table [Table 1]. The maps exhibit a stripe-like pattern, indicating the distribution of water and bilayer regions, with the former depicted by areas of high electron density and the latter by areas of low electron density. Consequently, low electron density bilayers are discernible as a one-dimensional periodic lamellar structure within the context of a high electron density water matrix.

3.1. Analysis of the L_α phase

The SAXS data pertaining to the L_α phase is examined by employing a methodology developed by Pabst et al. [19]. It should be emphasized that the L_α phase may be interpreted either through the convolution of the bilayer electron density profile with a series of parallel planes, each separated by a distance corresponding to the lamellar periodicity, or through the convolution of a bilayer with a set of one-dimensional lattice points, which are also spaced by distances that correspond to the lamellar periodicity. It is the initial interpretation that Pabst et al. adopt, with the objective of formulating a theory that clarifies the scattered intensity profile, which arises from the interaction between the L_α phase and X-rays of wavelength, λ, in conjunction with the scattering wavevector $q = \frac{4\pi\ Sin(\theta)}{\lambda}$, where 2θ denotes the scattering angle.

The Fourier transform of the electron density profile across the bilayer is designated as the form factor amplitude, represented by $f(q)$, whereas its squared value is directly proportional to this amplitude, referred to as the form factor, $F(q)$. In a similar manner, the Fourier transform of the array of parallel planes is identified as the structure factor amplitude, denoted as $s(q)$, and its squared value, recognized as the structure factor, $S(q)$, demonstrates a proportional relationship. Moreover, the scattered intensity, $I(q)$, from the observed structure is directly proportional to the product of the form factor, $F(q)$, and the structure factor, $S(q)$. The equation for the scattered intensity, $I(q)$, from the L_α phase is articulated as:

$$I(q) = scale[\frac{(1 - N_{dif})S(q)|f(q)|^2}{q} + \frac{N_{dif}|f(q)|^2}{q}] \tag{3}$$

The entire expression is subject to division by q, which signifies the denominator of the above equation [Equation (3)]. This factor is intricately connected to both the geometry of the detection apparatus used for data acquisition and the characteristics of the sample under examination. The specific configuration of the detector, characterized as being two-dimensional, along with the obtained SAXS patterns of the L_α phase (as well as disordered L_α phase), which are unoriented, leads to the conclusion that the determination of the geometric factor is equivalent to q. The $S(q)$ represents the structure factor associated with a series of parallel planes, whereas $f(q)$ indicates the amplitude of the form factor of the bilayer profile. The last element of equation [Equation (3)] relates to diffuse scattering, a phenomenon that is frequently overlooked when structural information is exclusively derived from Bragg peaks. In this regard, N_{dif} signifies the fraction of diffuse scattering.

The amplitude of the form factor, $f(q)$, is obtained through the Fourier transform of the electron density profile, represented as $\rho(z)$, across the bilayer, z represents the axis that is orthogonal to the bilayer plane. In the current situation, the stable and strongly correlated L_α phase is achieved when the molar ratio, α, is around 1; therefore, in this context, the cationic surfactant, CPC and anionic surfactant, SDS are jointly regarded as a catanionic molecule, and $\rho(z)$ can be described by five Gaussian functions, each representing different regions of this bilayer originating from the combined catanionic molecule [Fig. 9A]. The two Gaussian functions, symmetrically situated around the bilayer midpoint and relating to the head-groups of CPC molecules, are defined by a full width at half maxima (FWHM), σ_h, positioned at a distance $z = \pm z_h$ from the midpoint. The other two Gaussian functions, symmetrically arranged around the bilayer center and associated with the head-groups of SDS molecules, have a FWHM equal to σ_h, found at a distance $z = \pm z_m$ from the center. The fifth Gaussian function, representing the terminal methyl groups, is characterized by a FWHM value equal to σ_c at the midpoint of the bilayer ($z = 0$) [Fig. 9 A]. Therefore, the expression for $\rho(z)$ can be given as:

$$\begin{aligned}\rho(z) = \rho_{CH_2} + \rho_h\ [exp(-\frac{(z - z_h)^2}{2{\sigma_h}^2}) + exp(-\frac{(z + z_h)^2}{2{\sigma_h}^2})] + \\ \rho_m\ [exp(-\frac{(z - z_m)^2}{2{\sigma_m}^2}) + exp(-\frac{(z + z_m)^2}{2{\sigma_m}^2})] + \rho_c\ [exp(-\frac{z^2}{2{\sigma_c}^2})]\end{aligned} \tag{4}$$

In this scenario, the electron densities of the CPC head group, indicated by ρ_h, the SDS head group, marked as ρ_m, and the hydrocarbon tail, denoted as ρ_c, are calculated concerning the methylene electron density, represented by ρ_{CH_2}. This framework leads to the development of the

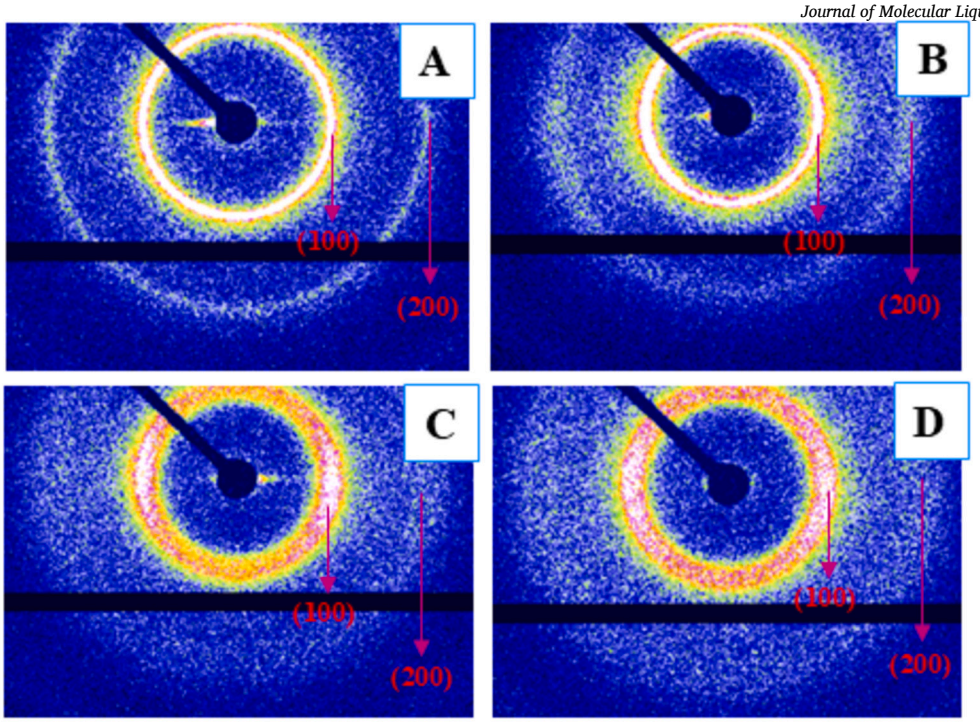

Fig. 7. Two-dimensional Small angle X-ray scattering data of the CPC-SDS-water of L_α phase of CPC-SDS-water system at $\Phi_s = 50$ & $T = 50\,°C$ and (A) $\alpha = 1.0$, (B) $\alpha = 1.2$, (C) $\alpha = 1.4$ and (A) $\alpha = 1.6$. The L_α phase found to be coexist with excess water.

form factor amplitude, $f(q)$ which is basically the Fourier transform of $\rho(z)$, can be shown as below.

$$f(q) = 2\sqrt{2\pi}\ \sigma_h\ \rho_h[exp(-\frac{{\sigma_h}^2 q^2}{2})]\ cos(qz_h)+ \\ 2\sqrt{2\pi}\ \sigma_m\ \rho_m[exp(-\frac{{\sigma_m}^2 q^2}{2})]\ cos(qz_m)+ \\ \sqrt{2\pi}\ \sigma c\ \rho_c\ [exp(-\frac{{\sigma_c}^2 q^2}{2})] \tag{5}$$

Moreover, pursuant to the modified Caille theory, the structure factor, $S(q)$ is defined as follows:

$$S(q) = N + 2\sum_{k=1}^{N-1}(N-k)cos(qkd) \times e^{-(d/2\pi)^2 q^2 \eta\gamma}\pi k^{-(d/2\pi)^2 q^2 \eta} \tag{6}$$

In this model, N represents the average number of coherent (correlated) scattering bilayers found in the stack. The constant γ denotes Euler's constant, whereas d indicates the lamellar periodicity. In addition, the parameter of Caille, represented by $\eta = (q^2 k_B\ B\ T)/(8\pi\sqrt{K\,B})$, includes the variables: K and B, which refer to the bending and bulk moduli, respectively, of the lamellar structure, while k_B denotes the Boltzmann constant. Model parameters like σ_h, σ_c, ρ_h, ρ_c, z_h, and η, along with N and N_{dif}, are adjusted to attain the best alignment between the observed and computed intensity profiles.

The SAXS pattern of the L_α phase, which is observed at $\alpha = 0.8$, $\Phi_s = 50$, and a temperature of $T = 50\,°C$, is beautifully depicted by this model. The information is depicted by a partially filled black diamond, with the fitting curve highlighted in red [Fig. 6(a)]. The electron density profile generated from the model is represented by the dotted red curve, comprising five Gaussians: two Gaussians corresponding to CPC head groups, illustrated by the cyan curve, two for SDS head groups, indicated by the pink curve, and one Gaussian for the alkyl terminal, shown in the blue curve [Fig. 9 A]. The identical electron density profile is depicted in the figure [Fig. 10a], and the associated model parameters are detailed in table [Table 2]. It should be noted that, the electron density distribution across the bilayer is shown concerning the electron density of the CH_2 group, which is arbitrarily set to zero and illustrated as a black, dashed line. The variation of the calculated form factor ($F(q) = f(q)^2$) is represented by a half-filled diamond symbol in black, while the structure factor ($S(q)$) is shown using the same diamond symbol in red, as illustrated in figure [Fig. 9B]. The structure factor shows two narrow peaks, while the form factor displays a more gradual change. It is important to mention that the theoretical intensity correlates directly with the multiplication of the form factor and structure factor.

Likewise, the SAXS patterns for the L_α phase, observed at $\alpha = 1.0$ and 1.2, $\Phi_s = 50$, at a temperature of $T = 50\,°C$, align well with the model [Fig. 6(b) & (c)]. The resulting electron density profile is illustrated in the figure [Fig. 10(b) & (c)], with the corresponding model parameters outlined in table [Table 2]. Additionally, the derived form factor and structure factor changes are presented in the figure [supporting Figure S2A] and [supporting Figure S2B], respectively. The changes in electron density profile along with form factor and structure factor are quite comparable for $\alpha = 0.8$ and $\alpha = 1.0$, but show differences when contrasted with $\alpha = 1.2$.

Notably, the CPC-SDS-water system at $\alpha = 1.4$ and 1.6 shows a short-range disordered L_α phase, with the SAXS pattern of this phase presenting a broad peak in the small angle region, unlike what is observed at $\alpha = 0.8$, 1.0, and 1.2. The occurrence of a broad peak in this phase could be due to the non-uniform stacking of the bilayers. Considering that the count of correlated bilayers, N, in the model for the L_α phase is a variable parameter, it can additionally help clarify the uneven stacking of bilayers. Consequently, we have used the same model of L_α phase with very low number of the correlated unit parameter, N, to characterize the SAXS data related to this short-range disordered L_α phase.

This model aligned notably with the SAXS pattern seen for the L_α phase at $\alpha = 1.4$ and 1.6, illustrated in figure [Fig. 6(d) & (e)], where the data is represented by half-filled diamonds in dark black, accompanied by the fit shown in yellow and purple curves, respectively. The table provided, referred to as [Table 2], details the relevant model parameters, whereas figure [Fig. 10(d) & (e)] depicts the electron density profiles derived from the analysis. The calculated form factor, denoted as $F(q)$ or $(f(q)^2)$, is illustrated in a half-filled diamond in black, while the structure factor ($S(q)$) is presented in a similar half-filled diamond symbol in red, as shown in figures [supporting Figure S2C] and [supporting Fig-

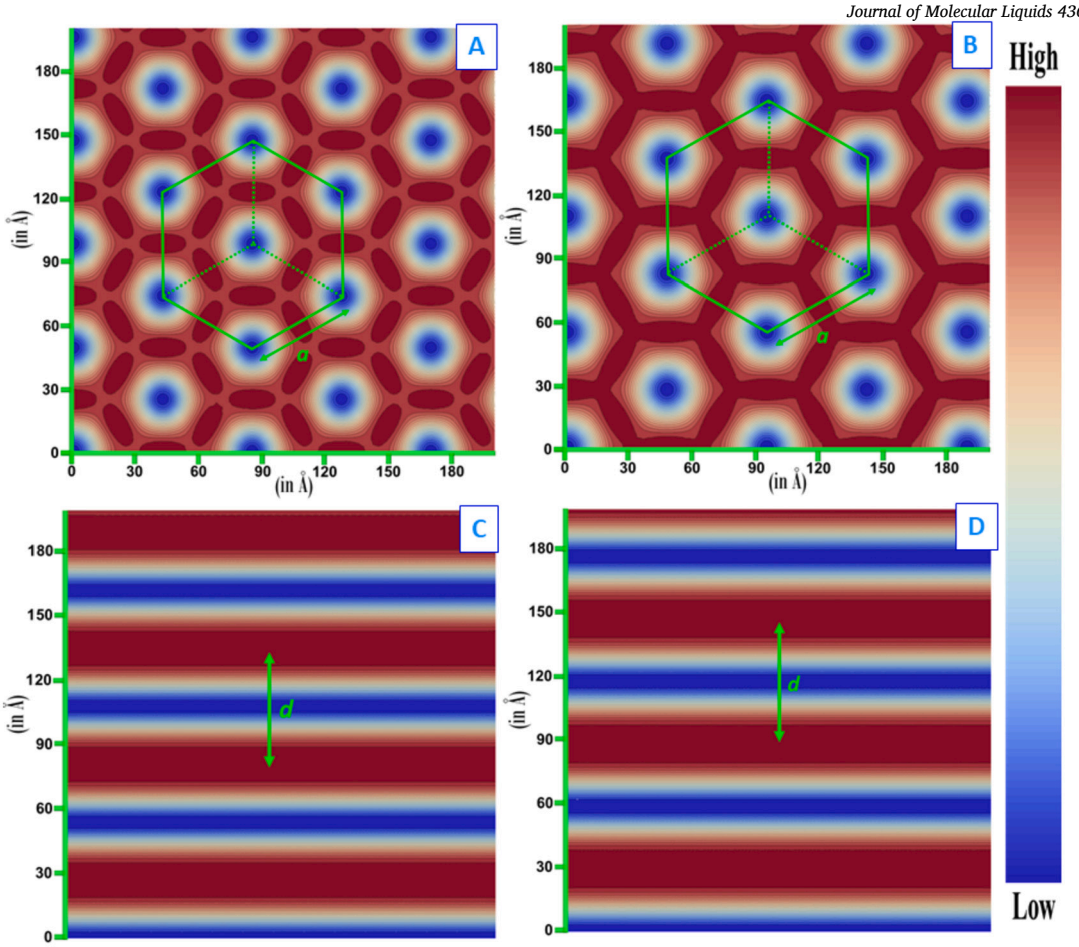

Fig. 8. Reconstructed electron density maps of the CPC-SDS-water system at $\Phi_s = 50$, $T = 50\,^{\circ}C$ and: (A) pure SDS system corresponding to the H, (B) $\alpha = 0.0$ (pure CPC system), corresponding to the H. Hexagon shows the conventional unit cell of the 2D hexagonal lattice and there are three primitive unit cells within this conventional unit cell. a is the lattice parameter. (C) $\alpha = 0.8$, corresponding to the L_α phase and (D) $\alpha = 1.0$, corresponding to the L_α phase. d is the lamellar periodicity. Deep red represents the highest electron density and deep blue is the lowest.

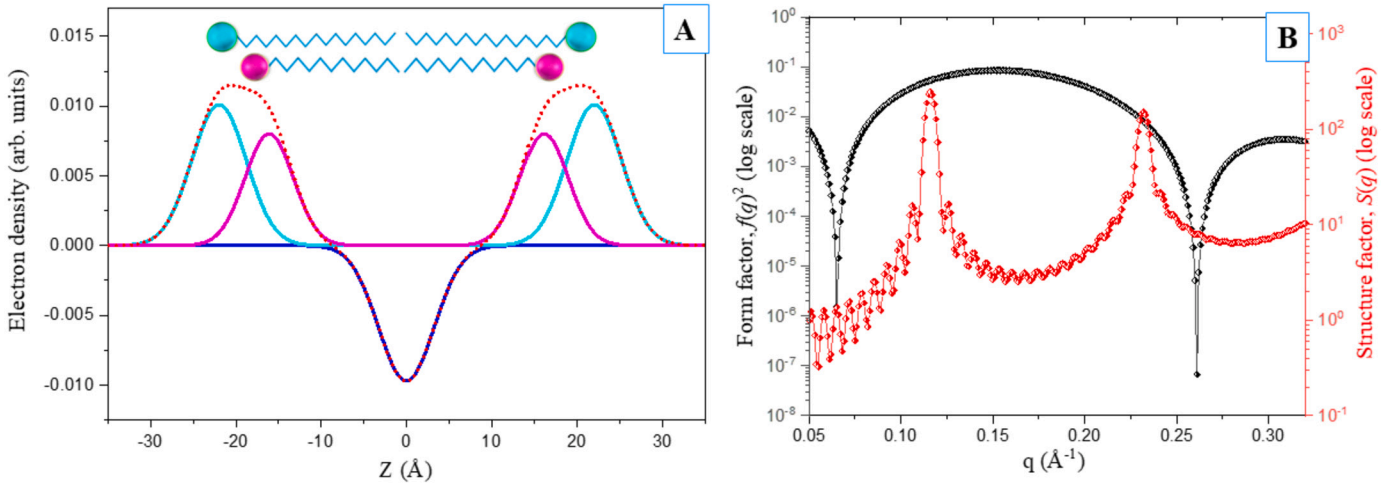

Fig. 9. (A) The bilayer profile contains the surfactant CPC hydrophilic head represented by a filled circle in cyan color and the surfactant SDS hydrophilic head indicated by a filled circle in pink color. The electron density profile across the bilayer comprises five Gaussians; two Gaussians are centered at the heads of the CPC molecule, represented by a curve in cyan color. Two Gaussians are centered at the heads of the SDS molecule, represented by a curve in pink color, and one Gaussian is centered at the center of the bilayer, as shown by the curve in blue color. The resultant electron density is represented by the dotted curve in red color, pertaining to the CPC-SDS-water system at $\alpha = 0.8$, $\Phi_s = 50$ and $T = 50\,^{\circ}C$. (B) The variation of the corresponding form factor ($F(q) = f(q)^2$) is illustrated using a half-filled diamond symbol in black coloration, while the structure ($S(q)$) is depicted in such a diamond symbol with red coloration for the CPC-SDS-water system at $\alpha = 0.8$, $\Phi_s = 50$ and $T = 50\,^{\circ}C$.

Table 2
Values of parameters obtained from the fit of the small angle X-ray scattering data at $\Phi_s = 50$ and $T = 50\,°C$ of the CPC-SDS-water system to the model of lamellar phase as described by Pabst et al. using five Gaussian profiles of the bilayer.

α	σ_h (Å)	σ_m (Å)	σ_c (Å)	$(\rho_c)/(\rho_h)$	$(\rho_c)/(\rho_m)$	z_h(Å)	z_m(Å)	η	N	N_{dif}	d (Å)	Phase
0.8	3.20	2.84	3.25	-0.96	-1.21	21.98	16.10	0.055	17	0	54.18	$I + L_\alpha$
1.0	3.40	2.96	3.24	-0.74	-1.19	23.65	17.50	0.055	14	0	59.13	$I + L_\alpha$
1.2	2.50	2.50	2.52	-1.0	-1.0	29.65	28.10	0.21	9	0.023	64.05	$I + L_\alpha$
1.4	2.56	2.50	3.04	-1.0	-1.0	27.65	26.40	0.14	3	0.039	57.5	$I + L_\alpha$
1.6	2.33	2.12	3.10	-1.0	-1.0	27.90	26.90	0.17	3	0.035	58.30	$I + L_\alpha$

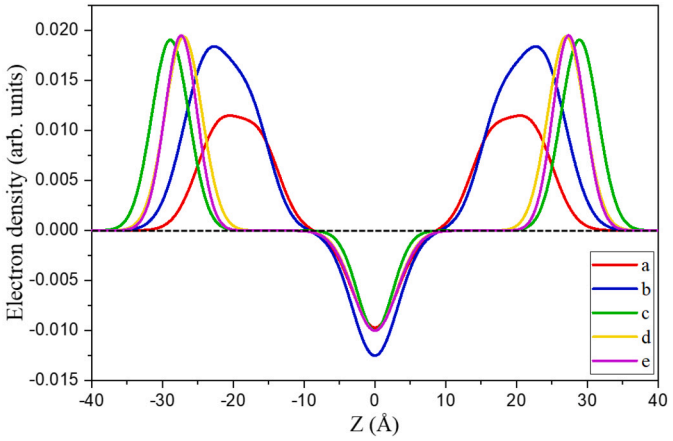

Fig. 10. Showing the variation of the electron density profile ($\rho(z)$) throughout the bilayer obtained from the parameters derived from the fitting of the model of L_α phase related to the CPC-SDS-water system at $\Phi_s = 50$, $T = 50\,°C$, and (a) $\alpha = 0.8$ is represented by the red curve, (b) $\alpha = 1.0$ is shown in blue, (c) $\alpha = 1.2$ is depicted in green, (d) $\alpha = 1.4$ is illustrated in yellow, and (e) $\alpha = 1.6$ is indicated by the purple curve. The electron density is illustrated concerning the electron density of the CH_2 group, which is assigned an arbitrary value of zero and shown as a black, dashed line. The z-axis is taken as normal to the bilayer plane.

ure S2D], respectively. On the other hand, the structure factor, together with the form factor, shows a wide and gradual change in relation to the scattering wave vector. The electron density profiles at $\alpha = 0.8$ and 1.0 are quite alike, while the profiles at $\alpha = 1.2$, 1.4, and 1.6 show a comparable trend but differ from those at $\alpha = 0.8$ and 1.0 [Fig. 10].

The elevated viscosity of the H phase noted in the pure CPC-water system ($\alpha = 0.0$) at $\Phi_s = 50$ and $T = 50\,°C$ suggests a potential formation of elongated worm-like micelles. This is due to the fact that, under such a high concentration of this surfactant in aqueous media, the configuration of cylindrical micelles transitions into worm-like micelles for entropic reasons, as micelles of cylindrical shape, regardless of their size, are unable to adequately occupy the available space. The emergence of these long, flexible micelles is ascribed to a reduction in the spontaneous curvature of the micelles, which in turn results in an elevation of the end-cap energy associated with the cylindrical micelles. This phenomenon is also quite prevalent in ionic surfactants when simple inorganic or organic salts are introduced [21,22] and bears a strong resemblance to the behavior observed in mixtures of cetyltrimethylammonium bromide (CTAB) with salts such as potassium bromide (KBr), sodium salicylate, sodium tosylate, and SHN [23], as well as in the cetylpyridinium bromide (CPB)-SHN-water system [24].

3.2. Analysis of the H phase

The H phase which is consisting of nearly monodisperse cylindrical micelles in solution, the corresponding SAXS scattering intensity $I(q)$ can be represented as the product of the form factor $F(q)$, which provides insights into the size and shape of the scattering cylindrical micelles, and the structure factor $S(q)$, which characterizes the interactions between particles. This can be expressed as follows.

$$I(q) = scale\ (\rho_{chain} - \rho_{water})^2\ F(q)\ S(q) \tag{7}$$

In this context, q represents the scattering wave vector, while ρ_{chain} denotes the electron density of the cylindrical micelle core, typically around 0.05 $e/Å^3$. Conversely, ρ_{water} refers to the electron density of water, which is generally about 0.334 $e/Å^3$. For elongated cylinders, the form factor, $F(q)$, can be effectively approximated as the product of the longitudinal factor, $Pl(q)$, and the cross-sectional scattering function, $Ps(q)$ [25]. The longitudinal factor can be considered as the form factor of an infinitely thin rod [26]. Consequently, $F(q)$ can be expressed as follows:

$$F(q) = Pl(q)\ Ps(q) \tag{8}$$

Here, $Pl(q)$ and $Ps(q)$ are given by the following relations:

$$Pl(q) = \frac{2}{q\ l}\left(\int_0^{q\ l} \frac{1}{t}\ sin(t)\ dt\right) - \frac{4\ sin^2(\frac{q\ l}{2})}{q^2\ l^2} \tag{9}$$

$$Ps(q) = \left(\frac{2\ J_1(q\ R)}{q\ R}\right)^2 \tag{10}$$

Consequently, by combining these two equations, the form factor, $F(q)$, can be expressed as follows:

$$F(q) = \left(\frac{2}{q\ l}\left(\int_0^{q\ l} \frac{1}{t}\ sin(t)\ dt\right) - \frac{4\ sin^2(\frac{q\ l}{2})}{q^2\ l^2}\right)\left(\frac{2\ J_1(q\ R)}{q\ R}\right)^2 \tag{11}$$

Here, R indicates the radius of the cylindrical micelles, and l signifies their length. Furthermore, J_1 is the Bessel function of the first kind. The structure factor, $S(q)$, is defined by the following relation [25]:

$$S(q) = 1 + (Z(q) - 1)G(q) \tag{12}$$

Where $Z(q)$ is given by the following relation.

$$Z(q) = c\frac{2}{a^2\ q}\sum_{hkl} m_{hkl}\ L_{hkl}(q) \tag{13}$$

In this instance, L_{hkl} refers to the peak shape functions that are positioned at the peak locations $q_{hkl} = \frac{4\pi}{a\sqrt{3}}\sqrt{h^2 + h\ k + k^2}$ and are identified by the Miller indices h, k, and l, while m_{hkl} signifies the multiplicity of the peak linked to the indices (hkl). The precise definitions of these peak shape functions are outlined as follows:

$$L_{hkl} = \frac{2}{\delta}\left|\frac{\Gamma[\frac{\nu}{2} + i\frac{\gamma_\nu 2(q - q_{hkl})}{(\pi\ \delta)}]}{\Gamma[\frac{\nu}{2}]}\right|^2 \tag{14}$$

with the imaginary unit i, the gamma function Γ, and

$$\gamma_\nu = \sqrt{\pi}\frac{\Gamma[\frac{\nu+1}{2}]}{\Gamma[\frac{\nu}{2}]} \tag{15}$$

In equations [Equation (14)] and [Equation (15)], the parameter ν plays a crucial role in defining the shape of the peak. When ν tends toward 0, the peak resembles a Lorentzian distribution, whereas it transitions to a Gaussian form as ν approaches infinity. The width of the peak is determined by the parameter δ, which is linked to the domain size, equivalent

to the correlation length ξ, as outlined earlier using the Debye-Scherrer equation.

$$\xi = 0.89\ \frac{2\pi}{\delta} \tag{16}$$

Additionally, $G(q)$ serves as the factor that accounts for the polydispersity of the cylinders and the lattice vibrations, expressed by the following relation:

$$G(q) = Exp[-q^2\ \Delta] \tag{17}$$

Where Δ contains the information about the width of the size distribution and lattice vibrations.

We have applied this model to analyze the SAXS pattern of the H phase. The SAXS pattern of the H phase, observed in pure SDS-water at a concentration of $\Phi_s = 50$ and a temperature of $T = 50\,°C$, is well characterized by this model. The SAXS data is represented by a half-filled black diamond, accompanied by the fitting curve in red, as illustrated in Figure [Fig. 3 A (a)]. The corresponding form factor and structure factor are displayed in [supporting Figure S3A]. The parameter δ, derived from the model, yields a correlation length that is consistent with previous calculations. Additionally, we have determined the radius of the cylindrical micelles to be approximately 17.72 $\mathring{A}$, which reflects the size of the SDS molecule. However, accurately measuring the size of SDS micelles in solution poses certain challenges. Nevertheless, both experimental findings and theoretical models indicate that the radius of these micelle spheres typically falls between 16 $\mathring{A}$ and 21 $\mathring{A}$, thus our derived value aligns with both theoretical and experimental results [27].

The SAXS pattern for the H phase, observed at $\alpha = 0$, $\Phi_s = 50$, and a temperature of $T = 50\,°C$, is accurately represented by this model. The SAXS data is depicted as a half-filled black diamond, accompanied by the fitting curve in blue, as illustrated in figure [Fig. 3 A (b)]. The corresponding form factor and structure factor are presented in figure [supporting Figure S3B]. The parameter δ, obtained from the model, provides a correlation length that aligns with earlier calculations. Furthermore, we have estimated the radius of the cylindrical micelles to be approximately 23.88 $\mathring{A}$, which corresponds to the size of the CPC molecule.

As noted, both surfactants, SDS and CPC, at $\Phi_s = 0$ and a temperature of 50 °C, are inclined to form the H phase. However, the incorporation of SDS into CPC at an α value of 0.2 results in the formation of the N_d phase, which occurs in proximity to the L_α^D phase, the latter being observed at $\alpha = 0.4$ and $\alpha = 0.6$. Furthermore, an increase in the concentration of SDS relative to CPC leads to a stable and positionally ordered L_α phase at α values of 0.8, 1.0, and 1.2. Nevertheless, a further increase in SDS concentration results in a disordered short-range L_α phase at α values of 1.4 and 1.6.

The size of the anionic surfactant, SDS, is shorter yet comparable to that of the cationic surfactant, CPC. Consequently, they combine to form a catanionic system when the value of α approaches 1, at which the shape factor of this catanionic molecule becomes nearly equal to 1, making it suitable for the formation of a bilayer structure. This phenomenon elucidates why the CPC-SDS-water system exhibits phase behavior for values of $\alpha = 0.8, 1.0$ and 1.2 that mimics that of an aqueous solution of double-charged lipid molecules, thereby exhibiting an ordered L_α phase. Such behavior accounts for the observed phase characteristics of the CPC-SDS-water system at these concentrations.

The incorporation of significantly shorter hydrotropes into surfactants is also recognized to promote the L_α phase over an extended range of Φ_s near $\alpha = 1$, indicating that SDS molecules in the CPC-SDS-water system behave similarly to hydrotropes. Hydrotropes are known to diminish the curvature of the water-oil interface. Therefore, for α values significantly exceeding 1, such as 1.4 and 1.6, where the number of SDS molecules is approximately 7 and 8 for every 5 CPC molecules, respectively, the curvature of the water-oil interface appears to be sufficiently reduced to introduce defects such as pores and channels in the L_α phase. These pores and channels exhibit a striking resemblance to dislocation loops. The influence of these dislocation loops has been investigated in relation to the smectic A - nematic liquid crystal transition, as proposed in the references [28,29], and theoretically, these loops are recognized to disrupt the quasi-long-range positional order of the smectic A phase. Consequently, the presence of such pores and channels in the current scenario appears to undermine the quasi-long-range positional order of the L_α phase, leading to the observation of a highly short-range disordered L_α phase.

In contrast, for values of α significantly below 1, such as 0.4 and 0.6, the number of SDS molecules present is approximately 4 and 6 for every 10 molecules of CPC, respectively. This indicates that about 40% to 60% of the CPC molecules are combined with SDS molecules to form catanionic structures, which a propensity to create bilayer formations. Meanwhile, the remaining CPC molecules have a tendency to spontaneously form spherical micelles, characterized by their highly curved structures, just above the critical micellar concentration. These two competitive effect, lead to the bilayer structures emerge alongside defects, such as holes filled with water, where the periphery of these holes accommodates additional CPC molecules in a curved configuration. Consequently, bilayers are formed, distinguished by randomly distributed holes of varying sizes, which ultimately arrange themselves into a lamellar structure. This process results in the emergence of a random mesh phase known as (L_α^D). Furthermore, in the case where α equals 0.2, the number of SDS molecules is limited to only 1 for every 5 molecules of CPC, meaning that only 20% of the CPC molecules contribute to the formation of catanionic molecules, suitable for bilayer formation and remaining CPC molecules like to form micelles with curved configurations which result as defect in the bilayers. As a consequence, the bilayers are unable to sustain a significant number of curved defects, leading to the formation of 'bicelles' (disk-like micelles) that establish a nematic phase (N_d).

The bilayers are primarily self-assembled to establish the L_α phase; nevertheless, they also possess the ability to generate isotropic phases, including the sponge (L_3) phase [30–32], which is characterized by steric repulsion, the dispersion of uni-lamellar vesicles (ULVs) [33], and the novel isotropic phase of the bilayer, which is noted for its short-range positional correlations and minimal average inter-bilayer spacing, predominantly influenced by attractive interactions [21,34,35]. Interestingly, the SDS and CPC are known to exhibit novel isotropic phase of bilayer in the presence of hydrotropes. For example, the surfactant SDS shows nematic phases of both rod and disk-shaped micelles, in addition to hexagonal and lamellar phases when PTHC is present [21,24,36,37]. Interestingly, the SDS-PTHC-water system shows a novel isotropic phase of the bilayer at elevated concentrations of PTHC [21]. On the other hand, CPC-SHN-water system demonstrates nematic phases of both types, including rod-like and disk-like, in addition to intermediate phases like ribbon, ordered mesh phases, random mesh structures, and lamellar phases when SHN is present. Additionally, the CPC-SHN-water system demonstrates a novel isotropic phase of the bilayer at increased concentrations of SHN [10,11,24]. Both systems are capable of forming the novel isotropic phase of the bilayers, however, the current CPC-SDS-water system displays hexagonal, nematic phases of disk-like micelles and lamellar structures; notably, it reveals a lamellar phase of short range order at increased SDS concentrations, suggesting a direct correlation between the observed short range (disordered) lamellar phase and the novel isotropic phase of the bilayer. In this case, the SDS molecule serves as an example of extreme hydrotropes with a long alkyl chain when compared to the hydrotropes PTHC and SHN. Moreover, it appears that extending the chain length of the hydrotropes can help to stabilize the disordered lamellar phase in comparison to the novel isotropic phase of the bilayers.

To study the swelling behavior of the bilayers in the lamellar phase, we have investigated the phase behavior of the CPC-SDS-water system at a molar ratio (α) of 0.9, with weight fractions (Φ_s) of 30, 39, 50, 60, 68, and 79, at a temperature of 50 °C. The system at Φ_s 30, 39, and 50 indicates the presence of excess water, while Φ_s 60, 68, and 79 do

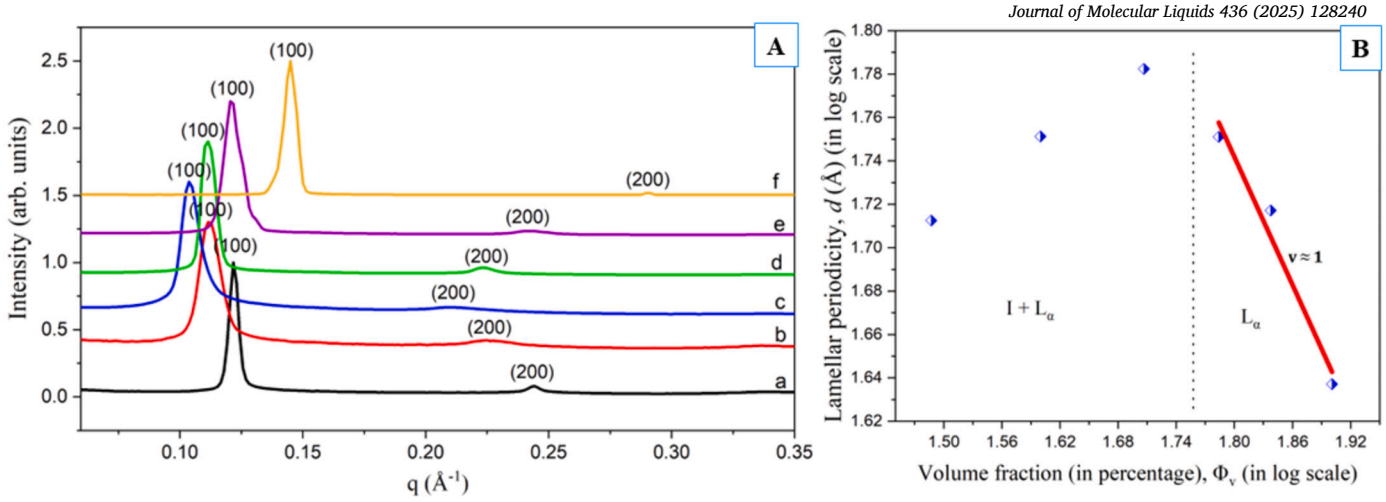

Fig. 11. Small angle X-ray scattering data of the CPC-SDS-water system at $\alpha = 0.9$ & T = 50 °C: (A) (a) $I + L_\alpha$ phase at $\Phi_s = 30$, (b) $I + L_\alpha$ phase at $\Phi_s = 39$, (c) $I + L_\alpha$ phase at $\Phi_s = 50$, (d) L_α phase at $\Phi_s = 60$, (e) L_α phase at $\Phi_s = 68$, and (f) L_α phase at $\Phi_s = 79$. (100) and (200) are the Miller indices of the first and second peaks of the X-ray diffraction pattern. (B) The variation of lamellar periodicity, d (expressed in logarithmic scale as $Log_{10}d$), in relation to the volume fraction (in percentage), Φ_v (also expressed in logarithmic scale as $Log_{10}\Phi_v$), is illustrated by a half-filled diamond in blue. This is accompanied by a linear fit represented as $Log_{10}d \sim -v\ Log_{10}\ \Phi_v$ with $v \sim 1$, depicted by a red curve in the pure L_α phase. I denote the isotropic phase due to excess of water.

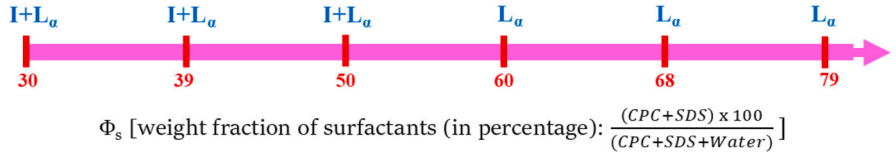

Fig. 12. Phase behavior of CPC-SDS-water system at molar ratio of $\frac{[SDS]}{[CPC]}$, $\alpha = 0.9$ (mole fraction of SDS, $\beta = 0.47$) & T = 50 °C: and various values of the weight fraction (in percentage), Φ_s. L_α and I denote the lamellar phase, and isotropic phase due to excess water, respectively.

not show any excess water. Nonetheless, all samples reveal oily streaks and maltese cross textures in POM under crossed polarizers [supporting Figure S4], which suggest the formation of the lamellar phase. The SAXS patterns for these samples exhibit two narrow quasi-Bragg peaks in the small angle region with a d-spacing ratio of $1 : \frac{1}{2}$, confirming the presence of the lamellar phase [Fig. 11A & supporting Figure S5]. The system at Φ_s 30, 39, and 50, which exhibit excess water, are categorized as $I + L_\alpha$, where I denotes the isotropic phase due to the excess water. Additionally, the phase corresponding to Φ_s 60, 68, and 79 is identified as L_α, as these samples do not contain excess water; the phase behavior is illustrated in the figure [Fig. 12]. The corresponding lamellar periodicity (lattice parameter), d, along with detailed indexing, is encapsulated in the table [supporting Table S1]. The swelling behavior, which denotes the variation of lamellar periodicity with Φ_s, is found to increase with rising Φ_s in the $I + L_\alpha$ phase, while it diminishes with increasing Φ_s in the L_α phase, as depicted by the half-filled diamond in blue in the figure [supporting Figure S6]. The same variation is also illustrated in terms of the volume fraction (in percentage) (Φ_v) in the figure [Fig. 11B]. Here, the volume fraction, Φ_v, is calculated from the weight fraction, Φ_s, by utilizing the mass densities of CPC, SDS, and $water$. The mass densities for CPC, SDS, and $water$ are considered to be $0.9362 g/cm^3$, $1.01 g/cm^3$, and $1 g/cm^3$, respectively. It has been observed that the system swells in the $I + L_\alpha$ phase, while it de-swell in the pure L_α phase. Furthermore, the swelling behavior of lamellar periodicity, d, in the pure L_α phase is described by the relationship $d \sim (\Phi_s)^v$ with $v \sim 1$. To illustrate this, we have presented the variation of the logarithm of lamellar periodicity, $Log_{10}d$, in relation to the logarithm of the volume fraction, $Log_{10}\Phi_v$ [Fig. 11B]. Thus, the swelling behavior of the pure L_α phase is characterized by $Log_{10}d \sim -vLog_{10}\Phi_v$ with $v \sim 1$, as depicted by the red curve in the figure [Fig. 11B], which aligns with the swelling behavior of bilayer structures.

The behavior of phase and aggregate morphology in mixtures of oppositely charged surfactants is well-documented to facilitate vesicle formation. For instance, the aqueous solution of cetyltrimethylammonium bromide (CTAB) and sodium octyl sulfate (SOS) demonstrates that the differing lengths of their hydrophobic chains promote the stabilization of vesicles compared to other microstructures, such as liquid crystalline and precipitate phases. This leads to the spontaneous formation of vesicles across a broad spectrum of compositions [38]. In a similar vein, when combining the single-chained cationic surfactant sodium dodecyl sulfate with the anionic surfactant dodecyltrimethylammonium bromide, the micelles of the anionic surfactant expand with the addition of the cationic surfactant. This results in a rapid transformation of rodlike micelles into vesicles within a very limited composition range [39]. In the current study, the aqueous solution of SDS and CPC also yields vesicles in comparison to other microstructures. Notably, this study reveals the emergence of a disordered lamellar phase at elevated α values, a phenomenon not previously observed in earlier systems.

4. Conclusion

In conclusion, the influence of sodium dodecyl sulfate (SDS), an anionic surfactant, on the phase behavior of cetylpyridinium chloride (CPC), a cationic surfactant, has been rigorously examined. Utilizing polarized optical microscopy (POM) and small-angle X-ray scattering (SAXS) techniques, we analyzed the CPC-SDS-water system at a temperature of $T = 50$ °C and a surfactant weight percentage $\Phi_s = 50$, while varying the molar ratio (α) of [SDS]/[CPC]. Our findings indicate that with an increase in SDS concentration, the system manifests distinct phases identified as H, N_d, $I + L_\alpha^D$, and $I + L_\alpha$.

For both H and L_α phases, electron density maps have been meticulously reconstructed. The map corresponding to the H phase illustrates the distribution of low electron density regions within a two-dimensional hexagonal lattice, whereas the map for the L_α phase reveals a lamellar arrangement of low electron density strips. The hexagonal H phase that was observed has been effectively matched with the theoret-

ical model. The model has allowed for the determination of the sizes of the SDS and CPC molecules, which are approximately 17.72 $\AA$ and 23.88 $\AA$, respectively, and these findings are consistent with previously published data.

Notably, the L_α phase at an α value near 1 demonstrates quasi-long-range positional order, while the L_α phase at higher SDS concentrations exhibits short-range positional order and is characterized as a disordered L_α phase. The occurrence of the L_α phase at both low and high α values has been thoroughly elucidated using the lamellar phase model proposed by Pabst et al. A distinctive aspect of the current study is our implementation of five Gaussian functions to represent the bilayer profile comprising CPC and SDS molecules, as opposed to the traditional three. Significantly, our results suggest that an increase in the chain length of the hydrotropes may contribute to stabilizing the disordered lamellar phase in contrast to the novel isotropic phase of the bilayers.

We have further elaborated on the phase behavior of the CPC-SDS-water system at $\alpha = 0.9$, T = 50^C, and Φ_s values of 30, 39, 50, 60, 68, and 79. The system at Φ_s 30, 39, and 50 exhibits an $I + L_\alpha$ phase, whereas the phase associated with Φ_s 60, 68, and 79 is classified as L_α. The swelling behavior of lamellar periodicity, d, in the pure L_α phase is represented by the relation ($d \sim (\Phi_s)^\upsilon$) with υ approximately equal to 1, which corresponds with the swelling behavior of bilayer structures.

In summary, our results may be of particular interest, especially in the context of developing carriers for drug delivery. This study serves as a catalyst for further experimental and theoretical investigations into the impact of the size of anionic surfactants/hydrotropes on the phase behavior of aqueous solutions containing cationic surfactants and vice versa.

CRediT authorship contribution statement

Mukesh Chandra Bos: Writing – original draft, Data curation, Conceptualization. **Shallu Dhingra:** Writing – original draft, Data curation, Conceptualization. **Manoj Kumar Srivastava:** Data curation, Conceptualization. **Priyanka Sharma:** Data curation, Conceptualization. **Santanu Kumar Pal:** Writing – review & editing, Visualization, Funding acquisition, Data curation, Conceptualization. **Santosh Prasad Gupta:** Writing – review & editing, Writing – original draft, Visualization, Methodology, Investigation, Funding acquisition, Data curation, Conceptualization.

Declaration of competing interest

The author declares that this article does not have a potential conflict of interest. This article also does not contain any studies with human or animal subjects.

Acknowledgements

S. P. Gupta expresses appreciation to Patna University for its technical assistance and funding (sanction order no.: 001/R&DC/RP/PU/Sanction dated 26/08/2023 (serial no. 6)). S. P. Gupta conveys gratitude to SERB-TARE (TAR/2021/000146) for the fellowship and the financial assistance provided. S. K. Pal extends thanks to SERB-TARE (TAR/2021/000146) for the financial assistance received. M. K. Srivastava expresses gratitude for the financial support received from the Higher Education Department of the Uttar Pradesh Government through the Research and Development scheme.

Appendix A. Supplementary material

Supplementary material related to this article can be found online at https://doi.org/10.1016/j.molliq.2025.128240.

Data availability

Data will be made available on request.

References

[1] J. Israelachvili, Intermolecular and Surface Forces, 2nd ed., Academic Press, London, 1991.
[2] R.G. Laughlin, The Aqueous Phase Behavior of Surfactants, Academic Press, London, 1994.
[3] N.A. Falk, Surfactants as antimicrobials: a brief overview of microbial interfacial chemistry and surfactant antimicrobial activity, J. Surfact Deterg 22 (2019) 1119–1127, https://doi.org/10.1002/jsde.12293.
[4] J.M. Seddon, R.H. Templer, in: R. Lipowsky, E. Sackmann (Eds.), Handbook of Biologicalphysics, Elsevier, Amsterdam, 1995.
[5] Book: Micelles, membranes, microemulsions, and monolayers, in: William M. Gelbart, Avinoam Ben-Shaul, Didier Roux (Eds.), Springer, 1994.
[6] S.T. Hyde, Interfacial architecture in surfactant-water mixtures: beyond spheres, cylinders and planes, Pure Appl. Chem. 64 (11) (1992) 1617–1622, https://doi.org/10.1351/pac199264111617.
[7] S.S. Funari, G. Rapp, A continuous topological change during phase transitions in amphiphile/water systems, PNAS 96 (14) (1999) 7756–7759, https://doi.org/10.1073/pnas.96.14.7756.
[8] S.K. Ghosh, R. Ganapathy, R. Krishnaswamy, J. Bellare, V.A. Raghunathan, A.K. Sood, Structure of mesh phases in a cationic surfactant system with strongly bound counterions, Langmuir 23 (2007) 3606–3614, https://doi.org/10.1021/la0631466.
[9] R. Zhou, M. Holmes, S. Puntambekar, M. Leaverd, R. McCabea, Hydrophobic counter ion effects on the formation of mesh and reversed phases in the perfluorodecanoate/water system, Soft Matter 8 (2012) 5835–5842, https://doi.org/10.1039/C2SM25295C.
[10] S.P. Gupta, V.A. Raghunathan, Controlling the thermodynamic stability of intermediate phases in a cationic-amphiphile–water system with strongly binding counterions, Phys. Rev. E 88 (2013) 012503, https://doi.org/10.1103/PhysRevE.88.012503, 1–10.
[11] S.P. Gupta, Thesis: Studies on novel phase behavior of ionic amphiphile-water systems, 2014.
[12] S.P. Gupta, Investigation of ordered mesh phases using their detailed reconstructed electron density maps, J. Mol. Liq. 315 (2020) 113831, https://doi.org/10.1016/j.molliq.2020.113831, 1–9.
[13] M.J. Rosen, X.Y. Hua, Synergism in binary mixtures of surfactants: II. some experimental data, J. Am. Oil Chem. Soc. 59 (1982) 582–585, https://doi.org/10.1007/BF02636329.
[14] A.W. Pochopien, P. Batys, J. Zawala, P.B. Kowalczuk, Synergistic effect of binary surfactant mixtures in two-phase and three-phase systems, J. Phys. Chem. B 125 (15) (2021) 3855–3866, https://doi.org/10.1021/acs.jpcb.1c00664.
[15] E. Kaler, A.K. Murthy, B.E. Rodriguez, J.A.N. Zasadzinski, Spontaneous vesicle formation in aqueous mixtures of single-tailed surfactants, Science 245 (4924) (1989) 1371–1374, https://doi.org/10.1126/science.2781283.
[16] T.F. Tadros, Self-Organized Surfactant Structures, 1st ed., Wiley-VCH, Germany, 2011.
[17] P. Kékicheff, B. Cabane, Between cylinders and bilayers: structures of intermediate mesophases of the sds/water system, J. Phys. 48 (9) (1987) 1571–1583, https://doi.org/10.1051/jphys:019870048090157100ff.
[18] J.F. Berret, D.C. Roux, G. Porte, Bisotropic-to-nematic transition in wormlike micelles under shear, J. Phys. II France 4 (1994) 1261–1279, https://doi.org/10.1051/jp2:1994198.
[19] G. Pabst, M. Rappolt, H. Amenitsch, P. Laggner, Structural information from multilamellar liposomes at full hydration: full q-range fitting with high quality X-ray data, Phys. Rev. E 62 (2000) 4000, https://doi.org/10.1103/PhysRevE.62.4000.
[20] S.P. Gupta, M. Gupta, S.K. Pal, Highly resolved morphology of room-temperature columnar liquid crystals derived from triphenylene and multialkynylbenzene using reconstructed electron density maps, ChemistrySelect 2 (21) (2017) 6070–6077, https://doi.org/10.1002/slct.201701117.
[21] M.C. Bos, S. Dhingra, M.K. Srivastava, P. Kumar, D. Kumar, S.K. Pal, S.P. Gupta, Effect of p-toluidine hydrochloride on the phase behavior of aqueous solution of sodium dodecyl sulfate, J. Mol. Liq. 416 (B) (2024) 126485, https://doi.org/10.1016/j.molliq.2024.126485.
[22] M.E. Cates, S.J. Candau, Statics and dynamics of worm-like surfactant micelles, J. Phys. Condens. Matter 2 (33) (1990) 6869, https://doi.org/10.1088/0953-8984/2/33/001.
[23] R. Krishnaswamy, S.K. Ghosh, S. Lakshmanan, V.A. Raghunathan, A.K. Sood, Phase behavior of concentrated aqueous solutions of cetyltrimethylammonium bromide (ctab) and sodium hydroxy naphthoate (shn), Langmuir 21 (23) (2005) 10439–10443, https://doi.org/10.1021/la051781q.
[24] S.K. Gosh, Thesis: Influence of strongly bound counterions on the phase behavior of ionic amphiphiles, 2007.
[25] A. Sundblom, C.L.P. Oliveira, A.E.C. Palmqvist, J.S. Pedersen, Modeling in situ small-angle X-ray scattering measurements following the formation of mesostructured silica, J. Phys. Chem. 113 (2009) 7706–7713, https://doi.org/10.1021/jp809798c.
[26] J.S. Pedersen, Analysis of small-angle scattering data from colloids and polymer solutions: modeling and least-squares fitting, Adv. Colloid Interface Sci. 70 (1997) 171–210, https://doi.org/10.1016/S0001-8686(97)00312-6.
[27] G. Duplâtre, M.F.F. Marques, M. da Graça Miguel, Size of sodium dodecyl sulfate micelles in aqueous solutions as studied by positron annihilation lifetime spectroscopy, J. Phys. Chem. 100 (41) (1996) 16608–16612, https://doi.org/10.1021/jp960644m.

[28] W. Helfrich, Defect model of the smectic a-nematic phase transition, J. Phys. France 39 (11) (1978) 1199–1208, https://doi.org/10.1051/jphys:0197800390110119900.

[29] R. Holyst, Dislocation loops in finite systems, Phys. Rev. B 50 (1994) 12398, https://doi.org/10.1103/PhysRevB.50.12398.

[30] S.P. Gupta, M. Thomas, A. Chowdhury, V.A. Raghunathan, Effect of adsorbed polyelectrolytes on the interactions and elasticity of charged surfactant bilayers, J. Phys. Condens. Matter 32 (2020) 194004, https://doi.org/10.1088/1361-648X/ab6d8d.

[31] G. Porte, J. Appell, P.B. et, J. Marignan, L to l3: a topology driven transition in phases of infinite fluid membranes, J. Phys. France 50 (1989) 1335–1347, https://doi.org/10.1051/jphys:0198900500110133500.

[32] D. Gazeau, A.M. Bellocq, D. Roux, T. Zemb, Experimental evidence for random surface structures in dilute surfactant solutions, Europhys. Lett. 9 (5) (1989) 447, https://doi.org/10.1209/0295-5075/9/5/007.

[33] D. Roux, C. Coulon, M.E. Cates, Sponge phases in surfactant solutions, J. Phys. Chem. 96 (11) (1992) 4174–4187, https://doi.org/10.1021/j100190a017.

[34] A. Pal, G. Pabst, V.A. Raghunathan, Defect-mediated lamellar-isotropic transition of amphiphile bilayers, Soft Matter 8 (2012) 9069–9072, https://doi.org/10.1039/C2SM26535D.

[35] A. Pal, P. Bharath, S.G. Dastidar, V.A. Raghunathan, Collapse and conservation of a lamellar phase by inter-headgroup bridging, Soft Matter 8 (2012) 927–930, https://doi.org/10.1039/C2SM06817F.

[36] S.K. Ghosh, V. Rathee, R. Krishnaswamy, V.A. Raghunathan, A.K. Sood, Re-entrant phase behavior of a concentrated anionic surfactant system with strongly binding counterions, Langmuir 25 (15) (2009) 8497–8506, https://doi.org/10.1021/la804330x.

[37] P.A. Hassan, S.R. Raghavan, E.W. Kaler, Microstructural changes in sds micelles induced by hydrotropic salt, Langmuir 18 (7) (2002) 2543–2548, https://doi.org/10.1021/la011435i.

[38] M.T. Yatcilla, K.L. HerringtonL, aura L. Brasher, E.W. Kaler, S. Chiruvolu, J.A. Zasadzinski, Phase behavior of aqueous mixtures of cetyltrimethylammonium bromide (ctab) and sodium octyl sulfate (sos), J. Phys. Chem. 100 (14) (1996) 5874–5879, https://doi.org/10.1021/jp952425r.

[39] K.L. Herrington, E.W. Kaler, Phase behavior of aqueous mixtures of dodecyltrimethylammonium bromide (dtab) and sodium dodecyl sulfate (sds), J. Phys. Chem. 97 (1993) 13792–13802.